

Northumbria Research Link

Citation: Tao, Xiang, Jin, Hao, Ma, Mengjuan, Quan, Liwei, Chen, Jinkai, Dong, Shurong, Zhang, He, Lv, Chaofeng, Fu, Yong Qing and Luo, Jikui (2019) Significantly Enhanced Performance of Triboelectric Nanogenerator by Incorporating BaTiO₃ Nanoparticles in Poly(vinylidene fluoride) Film. *Physica Status Solidi (a)*, 216 (7). p. 1900068. ISSN 1862-6300

Published by: Wiley-Blackwell

URL: <https://doi.org/10.1002/pssa.201900068> <<https://doi.org/10.1002/pssa.201900068>>

This version was downloaded from Northumbria Research Link:
<http://nrl.northumbria.ac.uk/id/eprint/38355/>

Northumbria University has developed Northumbria Research Link (NRL) to enable users to access the University's research output. Copyright © and moral rights for items on NRL are retained by the individual author(s) and/or other copyright owners. Single copies of full items can be reproduced, displayed or performed, and given to third parties in any format or medium for personal research or study, educational, or not-for-profit purposes without prior permission or charge, provided the authors, title and full bibliographic details are given, as well as a hyperlink and/or URL to the original metadata page. The content must not be changed in any way. Full items must not be sold commercially in any format or medium without formal permission of the copyright holder. The full policy is available online: <http://nrl.northumbria.ac.uk/policies.html>

This document may differ from the final, published version of the research and has been made available online in accordance with publisher policies. To read and/or cite from the published version of the research, please visit the publisher's website (a subscription may be required.)

Significantly Enhanced Performance of Triboelectric Nanogenerator by Incorporating BaTiO₃ Nanoparticles in Polyvinylidene Fluoride Film

Xiang Tao, Hao Jin^{}, Mengjuan Ma, Liwei Quan, Jinkai Chen, Shurong Dong, He Zhang, Chaofeng Lv, Yongqing Fu, Jikui Luo*

X. Tao, Prof. H. Jin, M. Ma, Prof. S. Dong
College of Information Science and Electronic Engineering, Zhejiang University, Hangzhou 310027, People's Republic of China
E-mail: hjin@zju.edu.cn

L. Quan, Prof. H. Zhang, Prof. C. Lv
College of Civil Eng. and Architecture, Zhejiang University, Hangzhou 310058, People's Republic of China

Prof. J. Luo
Institute of Renewable Energy and Environmental Technologies, Bolton University, Bolton BL3 5AB, United Kingdom

Prof. J. Chen
Ministry of Education Key Lab. of RF Circuits and Systems, College of Electronics & Information Hangzhou Dianzi University, Hangzhou 310018, People's Republic of China

Prof. Y. Fu
Faculty of Engineering and Environment, Northumbria University, Newcastle upon Tyne, NE1 8ST, United Kingdom

Keywords: triboelectric nanogenerators, polyvinylidene fluoride (PVDF), BaTiO₃ nanomaterial, high relative permittivity, high piezoelectric property

Abstract: Triboelectric nanogenerators (TENGs) have received significant attention in recent years due to their renewable and sustainable properties. They convert mechanical energy into electric energy through contact and separation of two dissimilar materials. Many methods have been developed to improve the performance of TENGs, but little attention has been paid to use nanoparticles such as BaTiO₃ (BTO) with a high dielectric constant for enhancing the performance. This paper reports the achievement of significant performance enhancement of polyvinylidene fluoride (PVDF)/polyamide-6 (PA6) TENGs by incorporating BTO nanoparticles into the PVDF film. The PVDF-BTO/PA6 TENG with 10 wt% BTO nanoparticles shows the best results with a peak voltage and charge density up to 900 V and

34.4 $\mu\text{C m}^{-2}$ at contact frequency of 5 Hz when the contact force and the spacer distance are 180 N and 100 mm, which are much higher than 384 V and 26.4 $\mu\text{C m}^{-2}$ of the PVDF/PA6 TENG without incorporating BTO nanoparticles. Further increase in the BTO concentration deteriorates the output performance of the TENGs. Detailed investigations on the piezo-response and permittivity of the PVDF-BTO films show that the increased piezoelectric constant and permittivity are responsible for the significantly enhanced performance of the TENGs. A mathematical model has been developed to describe the output voltages of the TENG as a function of thickness of the PVDF-BTO film.

1. Introduction

Triboelectric nanogenerators (TENGs), invented by Wang *et al.* in 2012,^[1] are a new type of nano-/micro-generators, and are able to convert a wide range of mechanical energies into usable electric energy through contact and separation of two dissimilar materials.^[1-4] As TENGs can produce very high output voltage and power with high efficiency, they have received much attention in recent years, particularly for the developments of renewable and sustainable energy.^[5-16] TENGs have been proven to be useful in developing self-powered intelligent electronic devices and systems, such as smart portable/wearable devices, wireless sensor networks and so on.^[4,17-19] There are four fundamental operation modes for TENGs: (i) the vertical contact-separation mode,^[20-26] (ii) the in-plane sliding mode,^[27-32] (iii) the single-electrode mode,^[33-38] and (iiii) the free standing triboelectric layer mode.^[39,40] They are simple in structures and fabrication, cost-effective, suitable for large-scale production^[41] with high output performance, and among them, the contact-separation mode is the most widely used due to its compactness, efficiency and high reliability.

Current development in this research field has been mainly focusing on enhancing the output performance of TENGs. Many methods, technologies and device structures have been

developed to enhance the performance of TENGs such as modulating surface roughness^[42–44] and nanoparticle dispersion^[20,45,46] to drastically increase the effective surface areas of contact materials; using ferroelectric and piezoelectric tribomaterials such as polyvinylidene fluoride (PVDF)^[47,48] and ZnO nanosheets^[49] to increase the surface charge density through polarization. Li *et al.*^[42] developed an effective surface modification method on the PET film, which realizes significant enhancement of triboelectric charge density for high-performance TENGs. Zhu *et al.*^[20] developed a new triboelectric nanogenerator using surface modifications with gold nanoparticles, and a peak short-circuit current of 2.0 mA was achieved, corresponding to an instantaneous power output of 1.2 W and a power density of 313 W m⁻². Whereas, such methods of nanoscale surface modification always need expensive equipments or complicated processes, which would lead to an increase in the cost of the TENGs. Jung *et al.*^[47] fabricated a hybrid generator which integrated a piezoelectric generator with a triboelectric generator, with a peak output voltage of ~370 V, a peak current density of ~120 mA m⁻², and a peak power density of ~4.44 mW cm⁻². Soin *et al.*^[48] demonstrated a significant increase in the output of PVDF/PA6 TENG by incorporating ZnSnO₃ nanoparticles in the PVDF polymer, with the voltage and current density increased from 300 V and 0.91 mA m⁻² to 520 V and 2.7 mA m⁻² respectively. Using piezoelectric tribomaterials can enhance the performance of TENGs via a combination of triboelectric and piezoelectric effects, and PVDF, owing to the presence of strong negative triboelectric properties and polarisation effect, is an excellent choice.

As the TENGs are capacitive type nanogenerators, increasing the relative permittivity of the triboelectric materials in contact can increase the capacitance of the device, and then more charges are induced and stored, thus improving the performance of the TENGs. There are some studies which can enhance output performance of TENGs by incorporating high dielectric nanoparticles into polydimethyl siloxane (PDMS) films.^[50,51] For example, Chen *et al.*^[50] designed an approach by filling the tribomaterial PDMS with high permittivity SrTiO₃

nanoparticles, and the voltage and current density have reached up to 305 V and $7.18 \mu\text{A cm}^{-2}$. Zhao *et al.*^[52] demonstrated a high output nanogenerator (NG) after adding high dielectric piezoelectric nanoparticles of BTO into the PVDF film, and produced a high voltage of 150 V, which was one of the best output performances among the lead-free NGs. However, their nanogenerator is belonged to the piezoelectric NGs whose working principle is different from that of the TENGs. As it can be seen that so far, most of the current researches in this respect have been focused on: the individual effects of increased surface areas or piezoelectricity caused by incorporating nanoparticles into the tribomaterials, and the effects of high permittivity of nanoparticles on the performance of TENGs. However one important issue about the combined effects of surface roughness, piezoelectric polarization and high permittivity have never been investigated yet, thus they deserve further studies in detail. This paper presents a TENG, consisting of a BTO-included PVDF (denoted as the PVDF-BTO hereafter) film as the negative tribomaterial, and a polyamide-6 (PA6) film as the positive tribomaterial. The PVDF piezoelectric film has better flexibility and piezo-electric performance,^[53] and incorporation of BTO nanoparticles in the PVDF film increases the relative permittivity, piezoelectric effect and surface roughness of the tribo-layer, and enhances the performance of the TENGs. The enhanced effect of the BTO nanoparticles on the performance of PVDF-BTO/PA6 TENGs has been investigated, and an optimized concentration is obtained. A mathematical model has been developed to describe the effect of PVDF-BTO film thickness on the output voltage of the TENG.

2. Results and discussions

2.1. Working principle of PVDF-BTO/PA6 TENG

The designed structure, a photo image and working principle of the PVDF-BTO/PA6 TENG are shown in **Figure 1a**, and the fabrication processes of the PVDF-BTO and PA6

films are illustrated in Figure 1b respectively. Two different sizes of glasses ($2\text{ cm} \times 2\text{ cm} \times 0.1\text{ cm}$ and $5\text{ cm} \times 5\text{ cm} \times 0.1\text{ cm}$) were used as the supporting substrates, and a conductive adhesive aluminum (Al) tape was glued on one side of the glass plates to act as the conductive electrode. The details of the fabrication processes for the PVDF-BTO and PA6 films are described in Experimental Section.

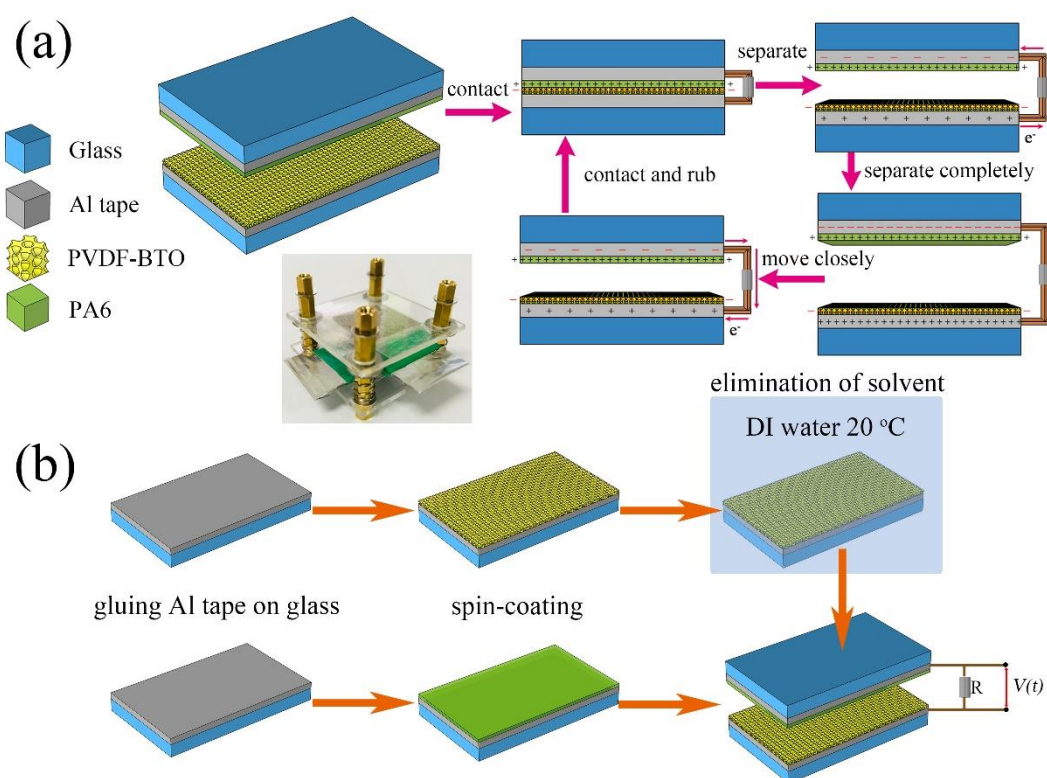


Figure 1. Illustration of a) device structure and working principle of the PVDF-BTO/PA6 TENG; b) fabrication processes for the PVDF-BTO and PA6 films.

Figure 1a schematically presents the working principle of the PVDF-BTO/PA6 TENG under the vertical compressive force. At start, two tribomaterials are separated by a distance, and there is no charge transfer. When a force is applied on one of the substrates, the two tribomaterials would contact each other, and electrons are injected from the PA6 film into the PVDF-BTO film due to different electron affinities, resulting in surface triboelectric

charges.^[50] When the two tribomaterials start to separate, the top PA6 electrode possess a higher electric potential than the bottom PVDF-BTO electrode, and the electrons would be driven from the bottom electrode to the top electrode through an external circuit. When the two tribomaterials are separated completely, the potential between the two electrodes is neutralized, and there is no further charge transfer. When the force is applied again, it shortens the separation, producing an electric potential difference with a reversed polarity.^[20] In consequence, electrons would be driven from the top electrode to the bottom electrode through the external circuit. When the contacting force is repeatedly applied, cyclic triboelectric charges will be generated, leading to an alternating current flow between the electrodes.

2.2. Performance of TENGs with different PVDF-BTO films

Using PVDF-BTO films of 36 μm thickness with different BTO concentrations, we have measured the output performance of PVDF-BTO/PA6 TENGs in order to find the optimal BTO concentration. In these experiments, the frequency and spacer distance of two tribo-plates were fixed at 5 Hz and 5 mm, respectively, and the contact force was changed from 20 N to 100 N with an incremental step of 20 N and the device size is fixed at $2 \times 2 \text{ cm}^2$. The output voltages of different PVDF-BTO/PA6 TENGs under different contact forces are shown in **Figure 2a**, and the obtained short-circuit currents are shown in **Figure 2b**. The corresponding current density and charge density were calculated and the results are shown in **Figure 2c** and **2d**, respectively.

As shown in **Figure 2a**, at a given contact force, the output voltage of PVDF-BTO/PA6 TENGs does not increase monotonically with the increase of BTO concentration, but increases firstly and then decreases with the further increase of the BTO concentration. Whereas, for all the PVDF-BTO/PA6 TENGs, the output voltage increases with the increase

of contact force monotonically. The variation trend of the short-circuit currents is similar to that of the output voltages. The curves of current densities, which are the ratios of peak current to plate area, are the similar to those of the short-circuit current curves. Furthermore, the charge density can be obtained by integrating the short-circuit current curve in one cyclic contact and separation period, and then being divided by the plate area. The charge density increases firstly and then decreases with the increase of the BTO concentration, but its variation with the BTO concentration is smoother than that of the short-circuit current. Obviously, the output voltage and short-circuit current reach to their maximum values at the 10% BTO concentration at any contact force, which means that 10% is the optimal BTO concentration in the experiments. When the contact force is 100 N, the peaks of output voltage and short-circuit current are 432 V and 13 μ A, respectively.

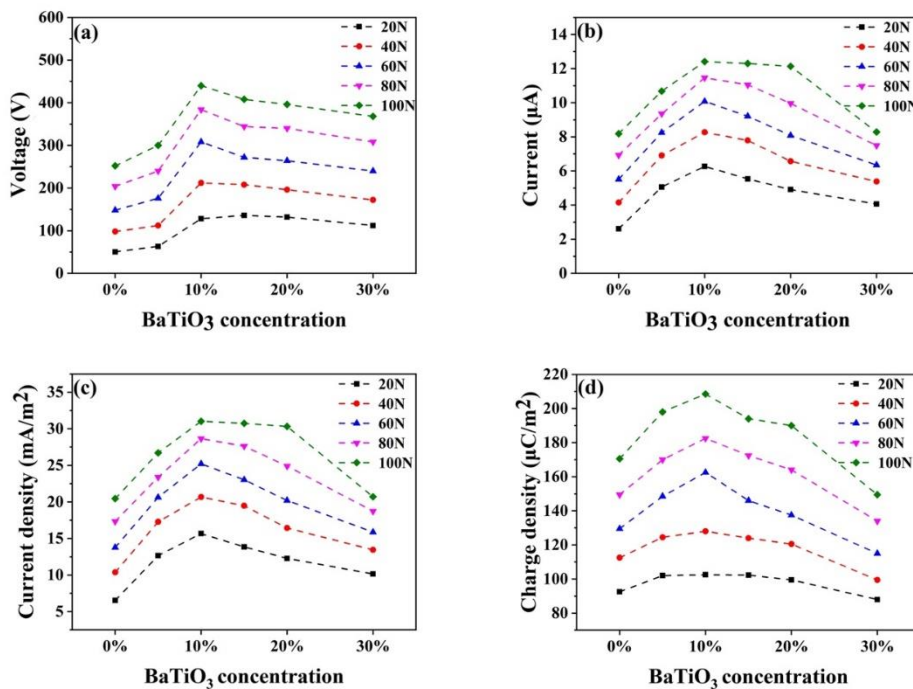


Figure 2. Output voltage (V_o) a), short-circuit current (I_{sc}) b), current density c) and charge density d) of PVDF-BTO/PA6 TENGs under different contact forces.

To further understand the effect of BTO on PVDF-BTO/PA6 TENGs' performance, the output performances of both the PVDF/PA6 TENG and PVDF-BTO/PA6 TENG with 10 wt% BTO concentration were investigated in details and the results are summarized in **Figure 3a-3f** for comparisons. In these experiments, the sizes of both types of devices were $5 \times 5 \text{ cm}^2$, and the thicknesses of all the PVDF-BTO films were $36 \text{ }\mu\text{m}$. The contact frequency was fixed at 5 Hz, while the contact force and the spacer distance were changed as variables. It can be seen from Figure 3a and 3b that the output voltages increase with the increase in both distance and contact force, and the output voltages of PVDF-BTO/PA6 TENG are much higher than those of PVDF/PA6 TENG at all the testing conditions. The peak voltages of both the PVDF/PA6 TENG and PVDF-BTO/PA6 TENG are shown in Figure 3c for comparison. The output voltage difference is increased with the increase of distance and contact force, and the output voltage of the PVDF-BTO/PA6 TENG is 900 V at 10mm/180N, more than twice of 384 V for the PVDF/PA6 TENG at the same testing conditions. The short-circuit currents of both the PVDF/PA6 TENG and PVDF-BTO/PA6 TENG are shown in Figure 3d and 3e, respectively. They are also increased with the increase in both distance and contact force, and the short-circuit currents of the PVDF-BTO/PA6 TENG are higher than those of the PVDF/PA6 TENG at all the test conditions. Figure 3f summarizes the differences in the charge densities between the PVDF/PA6 TENG and PVDF-BTO/PA6 TENG at different test conditions. Obviously, the output voltage, short-circuit current and charge density of the PVDF-BTO/PA6 TENG are all significantly larger than those of the pristine PVDF/PA6 TENG at all the test conditions, which means the output performance of the TENG has been significantly improved by adding the high dielectric constant material of BTO, with an optimal BTO concentration of 10 wt%.

The performance of the present TENG and the TENGs with porous PDMS films are summarized in **Table 1** for comparison. It can be seen from Table 1, the performance of

PVDF-BTO/PA6 TENG is pretty good, and the output voltage is superior to the TENGs with porous PDMS films.

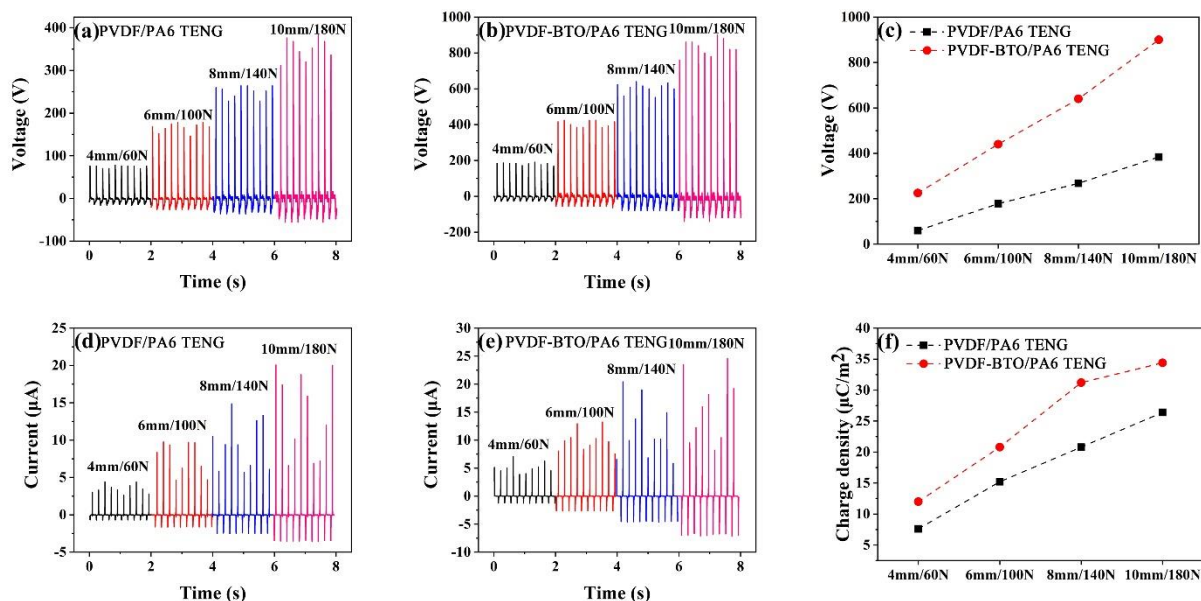


Figure 3. Comparisons of output voltages a, b, c), short circuit currents d, e) and charge densities f) for PVDF/PA6 TENG and PVDF-BTO/PA6 TENG. The devices were tested at a frequency of 5 Hz with different spacer distances and forces.

Table 1. Performance comparison between our TENG and those with porous PDMS films.

Reference	Doping material	output voltage [V]	current density [μA cm ⁻²]	charge density [nC cm ⁻²]
This paper	BTO	900	1	3.44
[54]	Au nanoparticles	220	2	0.25
[50]	SrTiO ₃	338	9.06	19
[55]	silver nanoparticles	400	7.5	24
[56]	carbon nanotubes	60	0.0288	6.5

The thickness of the PVDF-BTO films will influence the performance of the TENGs, and we have evaluated the output performance of the TENGs to find the optimal thickness by using PVDF-BTO films with various thicknesses. In these experiments, the frequency, spacer

distance, contact force and the size of two tribo-plates were fixed at 5 Hz, 5 mm, 100 N and $2 \times 2 \text{ cm}^2$ respectively, while the thicknesses of various PVDF-BTO films with 10 wt% BTO were varied to be 20 μm , 36 μm , 50 μm , 80 μm and 100 μm . The measured output voltages of different PVDF-BTO/PA6 TENGs using the PVDF-BTO films with various thicknesses are shown in **Figure 4a**, and the obtained short-circuit currents are shown in Figure 4b. The corresponding current densities and charge densities were further calculated, and the results are shown in Figure 4c and 4d, respectively.

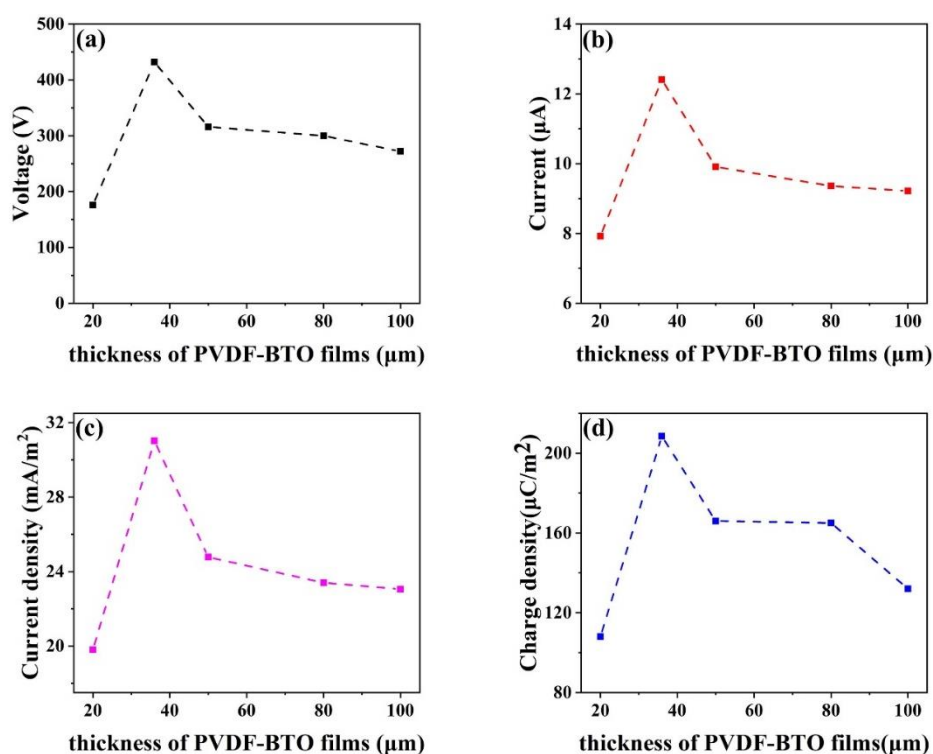


Figure 4. Output voltage (V_o) a), short-circuit current (I_{sc}) b), current density c) and charge density d) of PVDF-BTO/PA6 TENGs of various thicknesses.

As shown in Figure 4a, the output voltage of the PVDF-BTO/PA6 TENGs increases firstly and then decreases with the increase of PVDF-BTO film's thickness. Whereas the decreasing trend of the output voltage becomes flat when the thickness of PVDF-BTO film is

larger than 50 μm . The variation trends of the short-circuit currents and the current densities are similar to those of the output voltages. The charge density increases firstly and then decreases with the increase of PVDF-BTO film's thickness, but its variation with the PVDF-BTO film's thickness is much more significant than that of the short-circuit current.

Obviously, both the output voltage and short-circuit current achieve their maximum values at 36 μm , which mean that 36 μm is the optimal thickness of PVDF-BTO film for the TENG in our study.

2.3. Mechanism for high performance TENGs with additional BTO nanoparticles

Surface roughness, piezoelectric property and relative permittivity of the PVDF-BTO films with a fixed thickness of 36 μm but with various BTO concentrations were measured in order to investigate the mechanisms for the significant performance enhancement of the TENGs with additional BTO nanoparticles.

The surface morphologies of PVDF-BTO films with various BTO concentrations were characterized using the scanning electron microscope (SEM), and the results are shown in **Figure 5a–5f**. The pristine PVDF film has a much smoother surface with the lowest surface roughness, and the surface of the PVDF-BTO films becomes much rougher with the increase of the concentration of the BTO nanoparticles as can be seen in Figure 5b–5f. Furthermore, there are porous structures in the PVDF-BTO films after incorporated with the BTO nanoparticles in the PVDF. As the concentration of BTO nanoparticles is increased, more nanoparticles are dispersed inside the film, so that both the surface roughness and porosity of the film are increased. It can be also seen from Figure 5d–5f, when the BTO concentration is higher than 10 wt%, the nanoparticles have not been dispersed uniformly in the film, and some of them are agglomerated together, thus resulting in the increase of the size of the BTO clusters. The diameters of BTO clusters are in the range of 20–50 μm as shown in Figure 5d–

5f, and these BTO clusters would decrease the effective friction area of BTO/PVDF-BTO films compared to those with uniform distribution. The results show that the BTO nanoparticles are relatively well dispersed when the BTO concentration is less than 10 wt%.

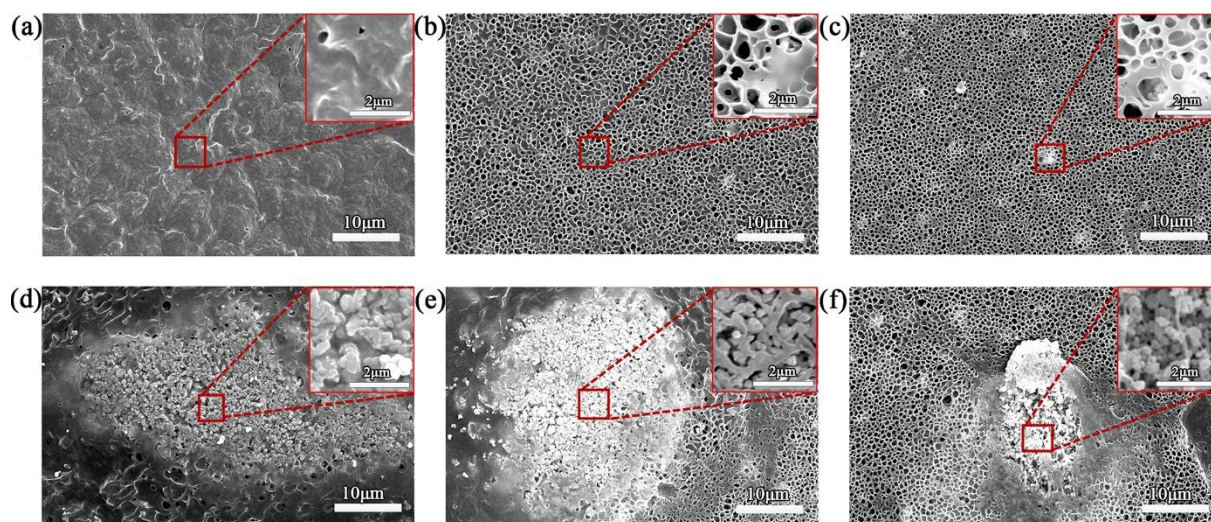


Figure 5. SEM images of the PVDF-BTO films with 0 wt% a) 5 wt% b), 10 wt% c), 15 wt% d), 20 wt% e), 30 wt% f) BTO nanoparticles.

Surface topographies of the PVDF-BTO films with various BTO concentrations before and after applied with the voltage were investigated using the piezoresponse force microscope (PFM), and the measurement results are shown in **Figure S1a–S1f** in the Supplementary Information (SI). The piezo-responses of the films were obtained by applying the voltage directly on the films. As shown in Figure S1, the brighter the region is, the larger the deformation it shows, and the darker region means that it is less deformed under the applied voltage.

The maximum deformation amplitude in the detected area of the PVDF-BTO film can be obtained from the measured results. The corresponding piezoelectric coefficient of the PVDF-BTO film can be calculated using the Equation (1):

$$d_{33} = \max(d) / V \quad (1)$$

Where d_{33} is the piezoelectric coefficient of PVDF-BTO films, $\max(d)$ is the maximum deformation in the measured area of the PVDF-BTO films, and V is the voltage applied. The calculated results are shown in **Figure 6**. The value of d_{33} for the pristine PVDF film is only 6 pm V^{-1} , smaller than those commonly reported for the commercial PVDF films, which are mostly due to the un-optimized synthesis process of the PVDF films. As the concentration of BTO is increased, the piezoelectric coefficient d_{33} of the film increases. However, when the BTO concentration is higher than 10 wt%, d_{33} begins to decrease. Hence, the d_{33} value reaches its peak value at the 10 wt% concentration of the BTO, and the maximum piezoelectric coefficient is 30 pm V^{-1} . This value is much higher than the typical d_{33} value ($\sim 26 \text{ pm V}^{-1}$) of the commercial PVDF films and 5 times of the pristine PVDF film synthesized by the same process, implying that the significantly enhanced piezoelectric properties can be achieved once the BTO nanoparticles are incorporated into the material. Since the BTO has better piezoelectric properties, the PVDF piezoelectric composite with the BTO as the active phase and the PVDF as the matrix exhibits excellent piezoelectric properties. However, when the BTO concentration is too high, the BTO powders cannot be dispersed uniformly in the film, and the BTO nanoparticles are agglomerated together as can be seen in Figure 5. As a consequence, the effects of BTO on the piezoelectric properties of the PVDF-BTO film becomes deteriorated, and thus its contribution to additional charge generation by polarization becomes decreased.

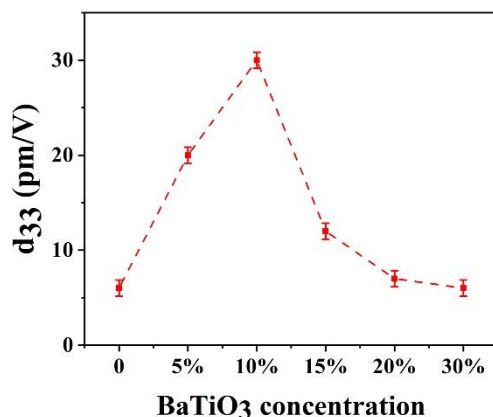


Figure 6. Piezoelectric coefficient of PVDF-BTO films with various BTO concentrations.

The relative permittivity of the PVDF-BTO films with various concentrations of the BTO was measured using an impedance analyzer, and the results are shown in **Figure 7a**. It can be seen that incorporation of BTO nanoparticles in the PVDF films has a significant effect on the relative permittivity of the PVDF-BTO films, and the relative permittivity hardly changes with the frequency when the frequency is larger than 100 Hz. In the experiments, the contact frequency of the TENGs was fixed at 5 Hz, and the results of the measured relative permittivity at 5 Hz for the PVDF-BTO films with different BTO concentrations are shown in **Figure 7b**. When the BTO concentration is 10 wt%, the relative permittivity of the PVDF-BTO film reaches its highest value of 20, which is about 60% increase as compared to that of the pristine PVDF (e.g., 12.5).

Theoretically, as the concentration of BTO is increased, the relative permittivity of PVDF-BTO films will be always increased,^[57] which is not the case for our obtained results. This is possibly due to the increased porosity/roughness of the films once the BTO concentration is higher than 10%, and the agglomeration of BTO nanoparticles can be evidenced from the SEM images shown in **Figure 5**. Because the TENG is a capacitive type device, the relative permittivity of the PVDF-BTO film will affect the capacitance of the TENG, hence the output performance.^[50]

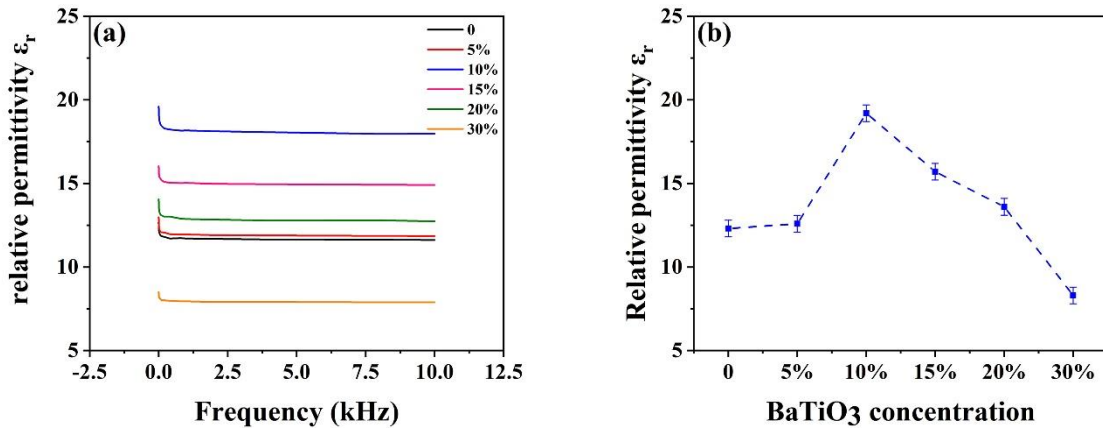


Figure 7. Relative permittivity of the PVDF-BTO films measured by an impedance analyzer over the frequency up to 10 kHz a), and relative permittivity of the PVDF-BTO films with various including densities at 5 Hz test frequency b).

Both the relative permittivity and piezoelectric constant are increased with the BTO concentration initially, and reach the maximum values at 10 wt% of the BTO concentration, then both of them decline with further increase in BTO concentration. The changes of both the permittivity and piezoelectric constant with the BTO concentration are coincided with the TENG's performance as shown in Figure 2, clearly indicating the significant contribution of the BTO nanoparticles to the enhanced performance of the TENGs, and the optimal BTO concentration in the PVDF films is about 10 wt%.

The PVDF-BTO films with 10 wt% BTO concentration but with different thicknesses were prepared by changing the spin coating parameters, and the obtained thicknesses were measured using a profilometer (D-100, KLA Tencor). The PVDF-BTO/PA6 TENG can be modeled using the $V-Q-x$ model,^[58] and a first-order ordinary differential equation was used to describe the relationship among transferred charges (Q), current (I) and voltage (V):

$$V = RdQ/dt = -Q(d_0 + x(t))/S\epsilon_0 + \sigma x(t)/\epsilon_0 \quad (2)$$

where R , t , ε_0 , $x(t)$, S and σ represent the external load resistance, time, vacuum permittivity, spacer distance, contact area and charge densities on the surface of PA6 film and PVDF-BTO film, respectively. R is the internal load resistance of the oscilloscope in our experiments, which is 100 M Ω . d_0 is the effective thickness of the TENG,^[58] which is expressed using Equation (3), where d_1 and d_2 are the thicknesses of the PA6 film and PVDF-BTO film, and ε_{r1} , ε_{r2} are the values of the relative permittivity of PA6 film and PVDF-BTO film. d_0 of the TENGs in our experiment is shown in **Table S1**, which can be expressed using:

$$d_0 = d_1 / \varepsilon_{r1} + d_2 / \varepsilon_{r2} \quad (3)$$

After introducing the boundary condition (when $t = 0$, $Q = 0$) to the Equation (2), we can derive the equations of $Q(t)$, $I(t)$, $V(t)$ and $V(t)/\sigma$, which are listed in the Equations (4) – (7).

$$Q(t) = \sigma S \left[1 - \exp\left(-\left(d_0 t + \int_0^t x(z) dz\right) / (RS\varepsilon_0)\right) \right] - \sigma d_0 \left(\int_0^t \exp\left(-d_0(t-\tau) / (RS\varepsilon_0) - \left(\int_\tau^t x(z) dz\right) / (RS\varepsilon_0)\right) d\tau \right) / (R\varepsilon_0) \quad (4)$$

$$I(t) = dQ/dt = -\sigma d_0 / (R\varepsilon_0) + \sigma (d_0 + x(t)) \exp\left(-\left(d_0 t + \int_0^t x(z) dz\right) / (RS\varepsilon_0)\right) / (R\varepsilon_0) + \sigma d_0 (d_0 + x(t)) \left(\int_0^t \exp\left(-d_0(t-\tau) / (RS\varepsilon_0) - \left(\int_\tau^t x(z) dz\right) / (RS\varepsilon_0)\right) d\tau \right) / (R^2 \varepsilon_0^2 S) \quad (5)$$

$$V(t) = RdQ/dt = -\sigma d_0 / \varepsilon_0 + \sigma (d_0 + x(t)) \exp\left(-\left(d_0 t + \int_0^t x(z) dz\right) / (RS\varepsilon_0)\right) / \varepsilon_0 + \sigma d_0 (d_0 + x(t)) \left(\int_0^t \exp\left(-d_0(t-\tau) / (RS\varepsilon_0) - \left(\int_\tau^t x(z) dz\right) / (RS\varepsilon_0)\right) d\tau \right) / (RS\varepsilon_0^2) \quad (6)$$

$$V(t)/\sigma = RdQ/(\sigma dt) = -d_0 / \varepsilon_0 + (d_0 + x(t)) \exp\left(-\left(d_0 t + \int_0^t x(z) dz\right) / (RS\varepsilon_0)\right) / \varepsilon_0 + d_0 (d_0 + x(t)) \left(\int_0^t \exp\left(-d_0(t-\tau) / (RS\varepsilon_0) - \left(\int_\tau^t x(z) dz\right) / (RS\varepsilon_0)\right) d\tau \right) / (RS\varepsilon_0^2) \quad (7)$$

When we study the relationship between the output performance of TENG and the thickness of PVDF-BTO film, ε_{r1} , ε_{r2} , d_1 , R , S are fixed in our experiments, and $x(t)$ is controlled by the operation program of the testing system. Therefore, the main variables that can affect the output performance of a TENG are the thickness of the PVDF-BTO film (d_2) and the charge densities on the surfaces of PA6 film and PVDF-BTO film (σ). According to Equation (7), V_{\max} / σ values for the TENGs with different effective thicknesses (d_0) can be obtained, and the results are shown in **Figure S2** in SI. Where V_{\max} is the peak value of the $V(t)$. As is shown in Figure S2, V_{\max} / σ is nearly a constant over the range of d_0 in our experiment, which means that the output voltage is roughly proportional to the charge density. Therefore, the variation trends of the output voltages and short-circuit currents are similar to those of the charge densities. As is shown in Figure 4d, the charge density increases firstly and then decreases with the further increase of the PVDF-BTO film's thickness. The possible explanation is that when the PVDF-BTO film is too thin, it is not conducive to charge storage, and when the film is too thick, it is not conducive to charge transfer. The optimal thickness of PVDF-BTO film is 36 μm in our experiment.

3. Conclusions

In summary, TENGs consist of a PVDF composite with incorporating high dielectric piezoelectric BTO nanoparticles (PVDF-BTO) and polyamide-6 (PA6) tribomaterials have been fabricated, characterized and analyzed in this paper. BTO is a material with high dielectric constant, which can increase the relative permittivity and piezoelectric effect of the PVDF-BTO film, thus enhancing the performance of the TENGs. Results show that the PVDF-BTO/PA6 TENG achieves its best performance when the concentration of the BTO is 10 wt% with the peak voltage and charge density of 900 V and 34.4 $\mu\text{C m}^{-2}$ respectively,

which are significantly higher than 384 V and $26.4 \mu\text{C m}^{-2}$ of the TENG with the pristine PVDF film. Moreover, a mathematical model of output voltage is derived to analyze the influences of the PVDF-BTO film's thickness on the TENGs' performance, and the theoretical analysis is in a good agreement with the measured results.

4. Experimental Section

4.1. Fabrication of TENGs

The fabrication processes of the PVDF-BTO and PA6 films are illustrated in Figure 1b. To obtain the PVDF-BTO films, PVDF solution was prepared by dissolving the PVDF powders in N,N-dimethylformamide (DMF) with a mass concentration of 20%; and the BTO powder was added in the PVDF solutions with concentrations of 5 wt%, 10 wt%, 15 wt%, 20 wt%, and 30 wt%, respectively, to obtain five different PVDF-BTO solutions. The PVDF-BTO solutions were stirred for 3 hrs at 70 °C, and then were spun coated onto the Al electrodes at 500 rpm for 10 s to spread the solutions, then 1000 rpm for 20 s to control the thickness. The PVDF-BTO films of different thicknesses were obtained by changing the spin coating parameters. The as-coated PVDF-BTO films were immersed immediately into deionized (DI) water at ~20 °C for 60 mins to completely eliminate the solvent,^[59] cleaned with DI water and dried overnight in air at room temperature. For a comparison, a PVDF film without adding the BTO nanoparticles was also fabricated using the same processes. The thicknesses of the PVDF-BTO films with various BTO concentrations and pristine PVDF film are about 36 μm , which were measured using a profilometer (D-100, KLA Tencor). To obtain PA6 films, a PA6 solution was prepared by dissolving the PA6 powders in the formic acid with a mass concentration of 20 wt%. The obtained solution was degassed, and then spun onto the Al electrode at 500 rpm for 10 s, then 1500 rpm for 20 s, and subsequently dried in an oven at 40 °C for 3 hrs. The thickness of PA6 films is about 60 μm . The scanning electron

microscope (SEM, S-4800, Hitachi) image and the X-Ray diffraction (XRD, EMPYREAN, PANalytical) pattern of the BTO nanoparticles are shown in **Figure S3a** and **S3b** in the Supplementary Information (SI), respectively. As shown in Figure S3, the maximum particle size of the BTO nanoparticles is less than 500 nm, and the BTO nanoparticles have six XRD peaks of (100), (110), (111), (200), (210), (211). The XRD peak splitting at $2\theta = \sim 45^\circ$ (Figure S3b) indicates that BTO nanoparticles are well-crystallized with a tetragonal phase.^[52]

4.2. TENG characterization setup

A dynamic fatigue tester (Popwil Model YPS-1) was used to characterize the TENGs by precisely controlling the contact force, frequency and spacer distance of two tribo-plates of different materials. An oscilloscope (Tektronix MDO3022) with an internal load resistance of 100 M Ω and a picoammeter (Keysight B2981A) were used to measure the output voltage (V_o) and short-circuit current (I_{sc}), respectively. For all the measurements, the electrode of PA6 side of the TENGs was connected to the positive side of the oscilloscope and picoammeter, with that of the PVDF side of TENGs grounded. In experiments, the dynamic fatigue tester system contacts the two plates under a fixed force before dynamic contact and separation. In a typical test, the plate consisting of the positive tribo-material was moved vertically to make contact with the plate with negative tribo-material. An impedance analyzer (Turnkey Concept 50, Novocontrol Technologies GmbH & Co. KG, Hundsangen, Germany), a piezoresponse force microscope (PFM, Cypher S D-100, Asylum Research) and the SEM were utilized to measure the relative permittivity, piezoelectric properties, and surface morphologies of the tribo-films, respectively.

Acknowledgements

This work was supported by the Zhejiang Province Key Research & Development Project (2018C01037); and Zhejiang Provincial Public Technology Research and Social Development Project (No. LGF19F010007), UK Engineering Physics and Science Research Council (EPSRC EP/P018998/1), Newton Mobility Grant (IE161019) through Royal Society and NFSC.

Received: ((will be filled in by the editorial staff))

Revised: ((will be filled in by the editorial staff))

Published online: ((will be filled in by the editorial staff))

References

- [1] F.-R. Fan, Z.-Q. Tian, Z. Lin Wang, *Nano Energy*. **2012**, *1*, 328.
- [2] W. Yang, J. Chen, G. Zhu, J. Yang, P. Bai, Y. Su, Q. Jing, X. Cao, Z.L. Wang, *ACS Nano*. **2013**, *7*, 11317.
- [3] G. Zhu, W.Q. Yang, T. Zhang, Q. Jing, J. Chen, Y.S. Zhou, P. Bai, Z.L. Wang, *Nano Lett.* **2014**, *14*, 3208.
- [4] X.S. Zhang, M.D. Han, R.X. Wang, F.Y. Zhu, Z.H. Li, W. Wang, H.X. Zhang, *Nano Lett.* **2013**, *13*, 1168.
- [5] P. Ding, J. Chen, U. Farooq, P. Zhao, N. Soin, L. Yu, H. Jin, X. Wang, S. Dong, J. Luo, *Nano Energy*. **2018**, *46*, 63.
- [6] J. Chen, J. Yang, Z. Li, X. Fan, Y. Zi, Q. Jing, H. Guo, Z. Wen, K.C. Pradel, S. Niu, Z.L. Wang, *ACS Nano*. **2015**, *9*, 3324.
- [7] Z.L. Wang, J. Chen, L. Lin, *Energy Environ. Sci.* **2015**, *8*, 2250.
- [8] J. Chen, Z.L. Wang, *Joule*. **2017**, *1*, 480.
- [9] G. Zhu, J. Chen, T. Zhang, Q. Jing, Z.L. Wang, *Nat. Commun.* **2014**, *5*, 3426.
- [10] J. Chen, Y. Huang, N. Zhang, H. Zou, R. Liu, C. Tao, X. Fan, Z.L. Wang, *Nat. Energy*. **2016**, *1*, 16138.
- [11] G. Zhu, Y.S. Zhou, P. Bai, X.S. Meng, Q. Jing, J. Chen, Z.L. Wang, *Adv. Mater.* **2014**, *26*, 3788.
- [12] G. Zhu, P. Bai, J. Chen, Z.L. Wang, *Nano Energy*. **2013**, *2*, 688.

- [13] J. Chen, G. Zhu, J. Yang, Q. Jing, P. Bai, W. Yang, X. Qi, Y. Su, Z.L. Wang, *ACS Nano*. **2015**, *9*, 105.
- [14] L. Zheng, G. Cheng, J. Chen, L. Lin, J. Wang, Y. Liu, H. Li, Z.L. Wang, *Adv. Energy Mater.* **2015**, *5*, 1501152.
- [15] Z. Lin, J. Chen, X. Li, Z. Zhou, K. Meng, W. Wei, J. Yang, Z.L. Wang, *ACS Nano*. **2017**, *11*, 8830.
- [16] J. Chen, J. Yang, H. Guo, Z. Li, L. Zheng, Y. Su, Z. Wen, X. Fan, Z.L. Wang, *ACS Nano*. **2015**, *9*, 12334.
- [17] B. Meng, W. Tang, X. Zhang, M. Han, W. Liu, H. Zhang, *Nano Energy*. **2013**, *2*, 1101.
- [18] B. Meng, W. Tang, Z. Too, X. Zhang, M. Han, W. Liu, H. Zhang, *Energy Environ. Sci.* **2013**, *6*, 3235.
- [19] A. Yu, M. Song, Y. Zhang, Y. Zhang, L. Chen, J. Zhai, Z.L. Wang, *Nano Res.* **2015**, *8*, 765.
- [20] G. Zhu, Z.H. Lin, Q. Jing, P. Bai, C. Pan, Y. Yang, Y. Zhou, Z.L. Wang, *Nano Lett.* **2013**, *13*, 847.
- [21] J. Chen, G. Zhu, W. Yang, Q. Jing, P. Bai, Y. Yang, T. Hou, Z.L. Wang, *Adv. Mater.* **2013**, *25*, 6094.
- [22] W. Yang, J. Chen, Q. Jing, J. Yang, X. Wen, Y. Su, G. Zhu, P. Bai, Z.L. Wang, *Adv. Funct. Mater.* **2014**, *24*, 4090.
- [23] J. Yang, J. Chen, Y. Liu, W. Yang, Y. Su, Z.L. Wang, *ACS Nano*. **2014**, *8*, 2649.
- [24] W. Du, X. Han, L. Lin, M. Chen, X. Li, C. Pan, Z.L. Wang, *Adv. Energy Mater.* **2014**, *4*, 1301592.
- [25] X. Fan, J. Chen, J. Yang, P. Bai, Z. L., Z.L. Wang, *ACS Nano*. **2015**, *9*, 4236.
- [26] W. Yang, J. Chen, G. Zhu, X. Wen, P. Bai, Y. Su, Y. Lin, Z.L. Wang, *Nano Res.* **2013**, *6*, 880.

- [27] S. Wang, L. Lin, Y. Xie, Q. Jing, S. Niu, Z.L. Wang, *Nano Lett.* **2013**, *13*, 2226.
- [28] G. Zhu, J. Chen, Y. Liu, P. Bai, Y.S. Zhou, Q. Jing, C. Pan, Z.L. Wang, *Nano Lett.* **2013**, *13*, 2282.
- [29] P. Bai, G. Zhu, Y. Liu, J. Chen, Q. Jing, W. Yang, J. Ma, G. Zhang, Z.L. Wang, *ACS Nano.* **2013**, *7*, 6361.
- [30] Z. Wen, J. Chen, M. Yeh, H. Guo, Z. Li, X. Fan, T. Zhang, L. Zhu, Z.L. Wang, *Nano Energy.* **2015**, *16*, 38.
- [31] Q. Jing, G. Zhu, P. Bai, Y. Xie, J. Chen, R.P.S. Han, Z.L. Wang, *ACS Nano.* **2014**, *8*, 3836.
- [32] S.Y. Kuang, J. Chen, X.B. Cheng, G. Zhu, Z.L. Wang, *Nano Energy.* **2015**, *17*, 10.
- [33] Z.L. Wang, *Faraday Discuss.* **2015**, *176*, 447.
- [34] Y. Yang, H. Zhang, Z.H. Lin, Y.S. Zhou, Q. Jing, Y. Su, J. Yang, J. Chen, C. Hu, Z.L. Wang, *ACS Nano.* **2013**, *7*, 9213.
- [35] Y. Yang, H. Zhang, J. Chen, Q. Jing, Y.S. Zhou, X. Wen, Z.L. Wang, *ACS Nano.* **2013**, *7*, 7342.
- [36] J. Yang, J. Chen, Y. Su, Q. Jing, Z. Li, F. Yi, X. Wen, Z. Wang, Z.L. Wang, *Adv. Mater.* **2015**, *27*, 1316.
- [37] Y. Yang, G. Zhu, H. Zhang, J. Chen, X. Zhong, Z.H. Lin, Y. Su, P. Bai, X. Wen, Z.L. Wang, *ACS Nano.* **2013**, *7*, 9461.
- [38] Y. Su, G. Zhu, W. Yang, J. Yang, J. Chen, Q. Jing, Z. Wu, Y. Jiang, Z.L. Wang, *ACS Nano.* **2014**, *8*, 3843.
- [39] S. Wang, Y. Xie, S. Niu, L. Lin, Z.L. Wang, *Adv. Mater.* **2014**, *26*, 2818.
- [40]- H. Guo, J. Chen, M.H. Yeh, X. Fan, Z. Wen, Z. Li, C. Hu, Z.L. Wang, *ACS Nano.* **2015**, *9*, 5577.
- [41] R.G. Horn, D.T. Smith, *Science (80-.)*. **1992**, *256*, 362.

- [42] H.Y. Li, L. Su, S.Y. Kuang, C.F. Pan, G. Zhu, Z.L. Wang, *Adv. Funct. Mater.* **2015**, 25, 5691.
- [43] S. Lee, Y. Lee, D. Kim, Y. Yang, L. Lin, Z.H. Lin, W. Hwang, Z.L. Wang, *Nano Energy*. **2013**, 2, 1113.
- [44] X.S. Zhang, M. Di Han, R.X. Wang, B. Meng, F.Y. Zhu, X.M. Sun, W. Hu, W. Wang, Z.H. Li, H.X. Zhang, *Nano Energy*. **2014**, 4, 123.
- [45] G. Wang, Y. Xi, H. Xuan, R. Liu, X. Chen, L. Cheng, *Nano Energy*. **2015**, 18, 28.
- [46] X. He, H. Guo, X. Yue, J. Gao, Y. Xi, C. Hu, *Nanoscale*. **2015**, 7, 1896.
- [47] W.S. Jung, M.G. Kang, H.G. Moon, S.H. Baek, S.J. Yoon, Z.L. Wang, S.W. Kim, C.Y. Kang, *Sci. Rep.* **2015**, 5, 9309.
- [48] N. Soin, P. Zhao, K. Prashanthi, J. Chen, P. Ding, E. Zhou, T. Shah, S.C. Ray, C. Tsonos, T. Thundat, *Nano Energy*. **2016**, 30, 470.
- [49] A.A. Narasimulu, P. Zhao, N. Soin, K. Prashanthi, P. Ding, J. Chen, S. Dong, L. Chen, E. Zhou, C.D. Montemagno, *Nano Energy*. **2017**, 40, 471.
- [50] C. Jie, H. Guo, X. He, G. Liu, X. Yi, H. Shi, C. Hu, *ACS Appl. Mater. Interfaces*. **2016**, 8, 736.
- [51] Z. Fang, K.H. Chan, X. Lu, C.F. Tan, G.W.W. Ho, *J. Mater. Chem. A*. **2017**, 6, 52.
- [52] Y. Zhao, Q. Liao, G. Zhang, Z. Zhang, Q. Liang, X. Liao, Y. Zhang, *Nano Energy*. **2015**, 11, 719.
- [53] T. Cheng, X. Fu, W. Liu, X. Lu, X. Chen, Y. Wang, G. Bao, *Renew. Energy*. **2019**, 135, 399.
- [54] J. Chun, J.W. Kim, W. Jung, C. Kang, S. Kim, Z.L. Wang, J.M. Baik, *Energy Environ. Sci.* **2015**, 8, 3006.
- [55] X. Xia, J. Chen, H. Guo, G. Liu, D. Wei, Y. Xi, X. Wang, C. Hu, *Nano Res.* **2017**, 10, 320.

- [56] Y.J. Fan, X.S. Meng, H.Y. Li, S.Y. Kuang, L. Zhang, Y. Wu, Z.L. Wang, G. Zhu, *Adv. Mater.* **2017**, *29*, 1603115.
- [57] T. Yamada, T. Ueda, T. Kitayama, *J. Appl. Phys.* **1982**, *53*, 4328.
- [58] S. Niu, S. Wang, L. Lin, Y. Liu, Y. Zhou, Y. Hu, Z. Wang, *Energy Env. Sci.* **2013**, *6*, 3576.
- [59] N. Soin, D. Boyer, K. Prashanthi, S. Sharma, A.A. Narasimulu, J. Luo, T.H. Shah, E. Siores, T. Thundat, *Chem. Commun.* **2015**, *51*, 8257.

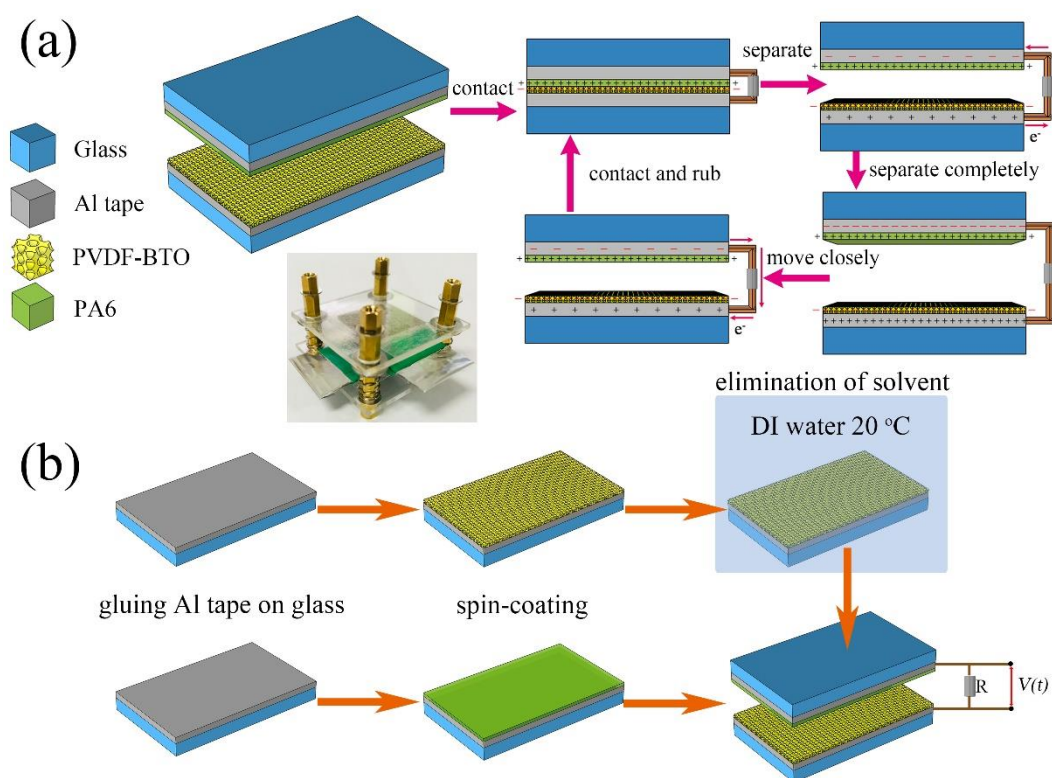


Figure 1. Illustration of a) device structure and the working principle of the PVDF-BTO/PA6 TENG; b) fabrication processes for the PVDF-BTO and PA6 films.

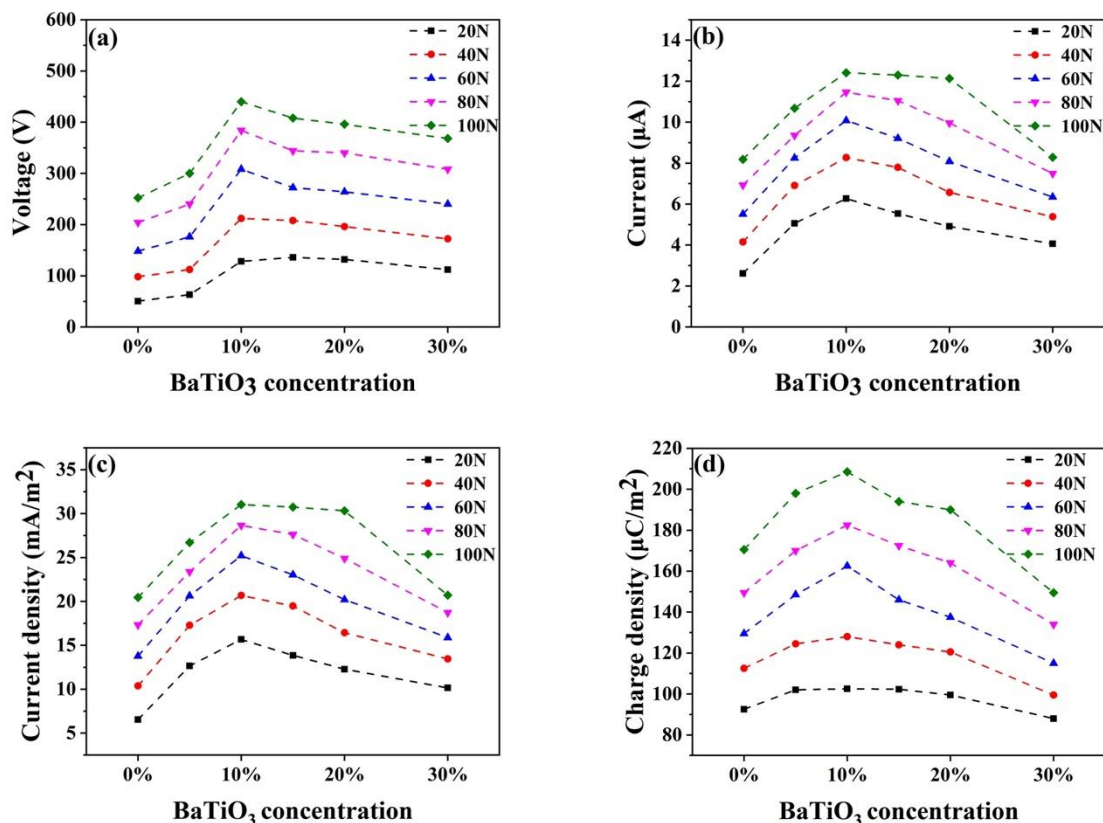


Figure 2. Output voltage (V_o) a), short-circuit current (I_{sc}) b), current density c) and charge density d) of PVDF-BTO/PA6 TENGs under different contact forces.

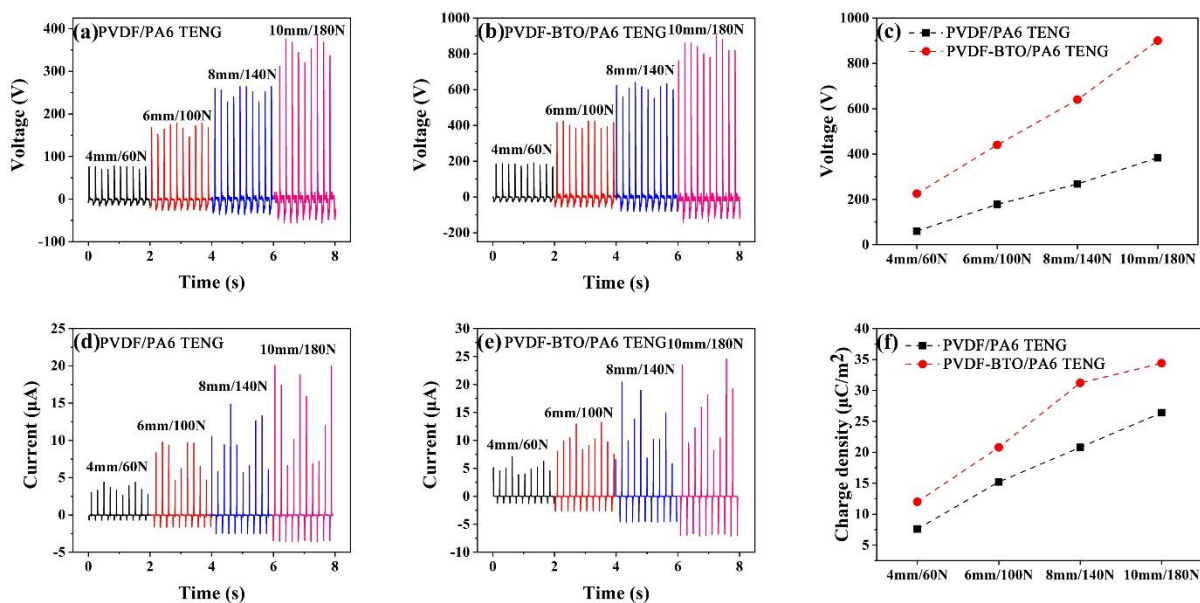


Figure 3. Comparisons of output voltages a, b, c), short circuit currents d, e) and charge densities f) for PVDF/PA6 TENG and PVDF-BTO/PA6 TENG. The devices were tested at a frequency of 5 Hz with different spacer distances and forces.

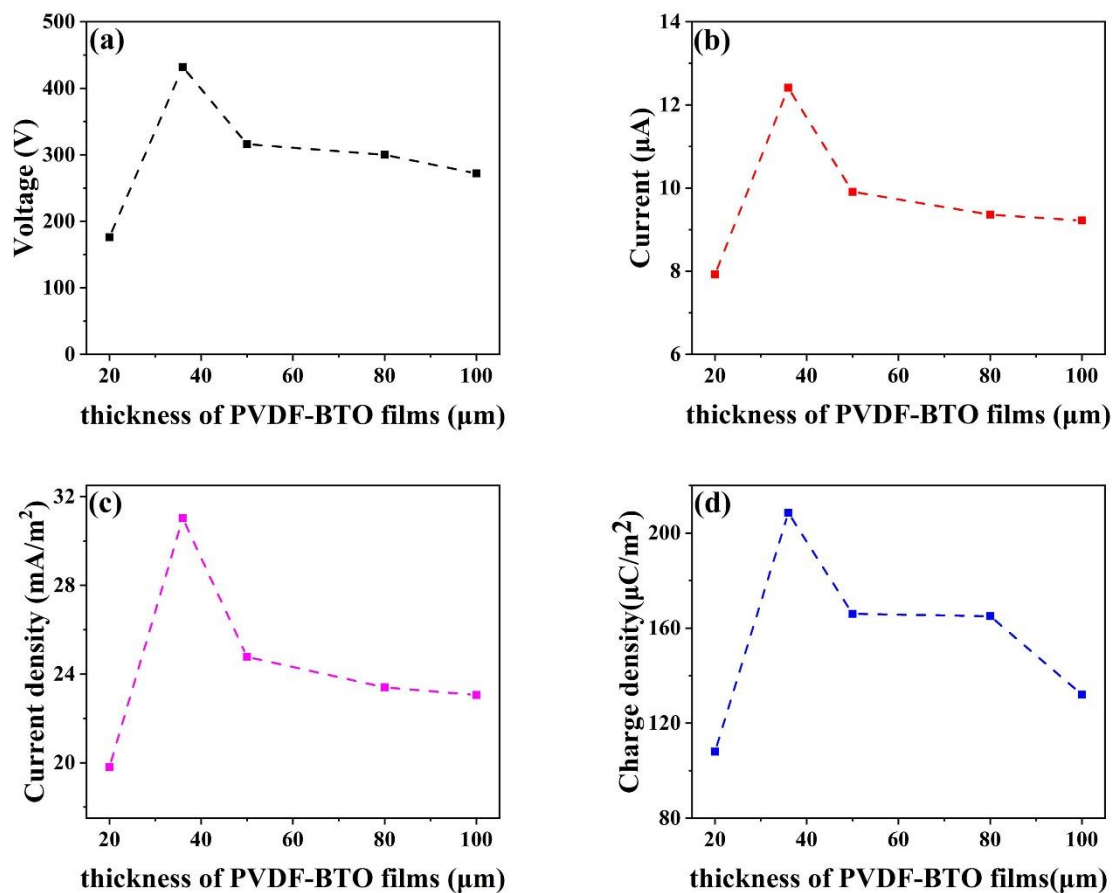


Figure 4. Output voltage (V_o) a), short-circuit current (I_{sc}) b), current density c) and charge density d) of PVDF-BTO/PA6 TENGs of various thicknesses.

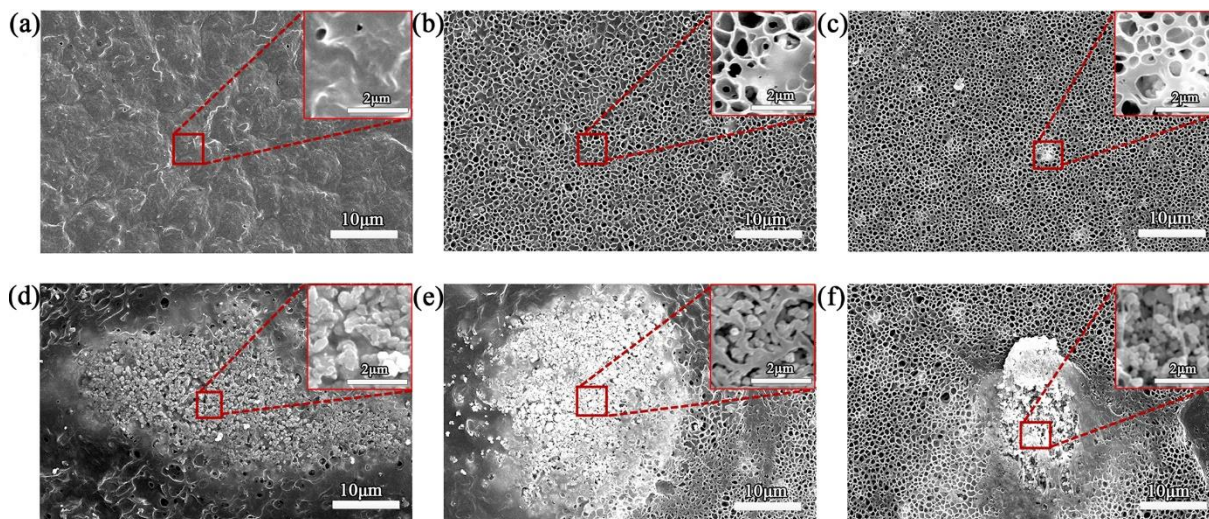


Figure 5. SEM images of the PVDF-BTO films with 0 wt% a) 5 wt% b), 10 wt% c), 15 wt% d), 20 wt% e), 30 wt% f) BTO nanoparticles.

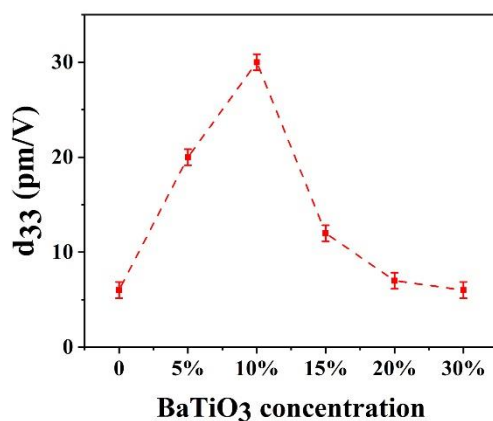


Figure 6. Piezoelectric coefficient of PVDF-BTO films with various BTO concentrations.

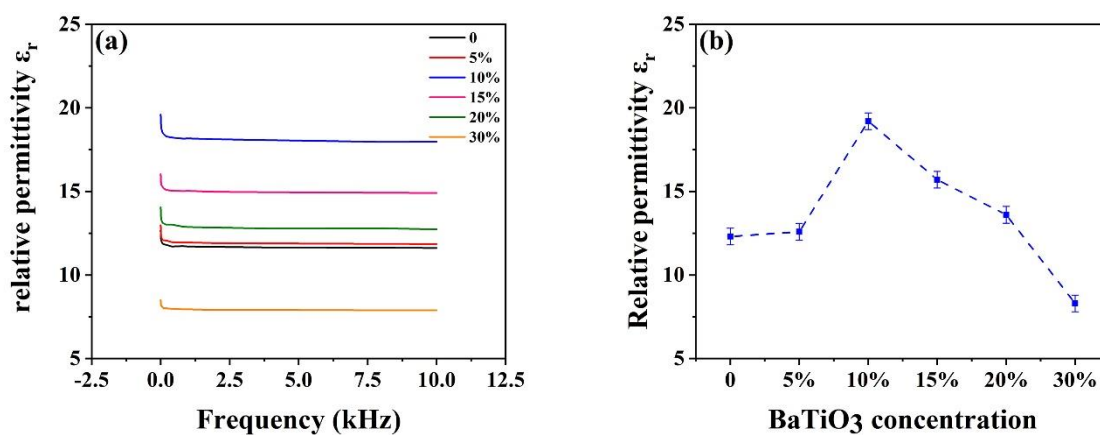


Figure 7. Relative permittivity of the PVDF-BTO films measured by an impedance analyzer over the frequency up to 10 kHz a), and relative permittivity of the PVDF-BTO films with various including densities at 5 Hz test frequency b).

Table 1. The output performance comparison between the present TENG and the TENGs with porous PDMS films.

Reference	Doping material	output voltage	current density	charge density
		[V]	[$\mu\text{A cm}^{-2}$]	[nC cm ⁻²]
This paper	BTO	900	1	3.44
[54]	Au nanoparticles	220	2	0.25
[50]	SrTiO ₃	338	9.06	19
[55]	silver nanoparticles	400	7.5	24
[56]	carbon nanotubes	60	0.0288	6.5

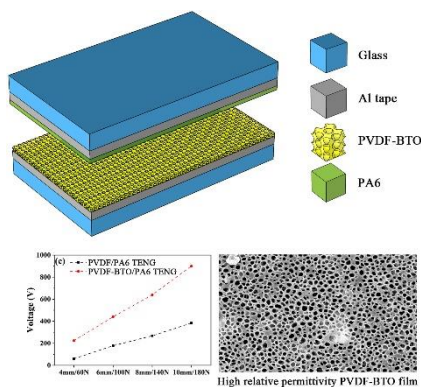
The table of contents: Incorporation of BaTiO₃ (BTO) nanoparticles in PVDF enhances the performance of triboelectric nanogenerators (TENGs). The PVDF-BTO/PA6 TENG with 10 wt% BTO shows the best results with a peak voltage and charge density up to 900 V and 34.4 $\mu\text{C m}^{-2}$ respectively, much higher than 384 V and 26.4 $\mu\text{C m}^{-2}$ of the PVDF-PA6 TENG without BTO nanoparticles.

Keyword triboelectric nanogenerators, polyvinylidene fluoride (PVDF), BaTiO₃ nanomaterial, high relative permittivity, high piezoelectric property

X. Tao, H. Jin^{*}, M. Ma, L. Quan, J. Chen, S. Dong, H. Zhang, C. Lv, Y. Fu, J. Luo

Significantly Enhanced Performance of Triboelectric Nanogenerator by Incorporating BaTiO₃ Nanoparticles in Polyvinylidene Fluoride Film

ToC figure



Copyright WILEY-VCH Verlag GmbH & Co. KGaA, 69469 Weinheim, Germany, 2018.

Supporting Information

Significantly Enhanced Performance of Triboelectric Nanogenerator by Incorporating BaTiO₃ Nanoparticles in Polyvinylidene Fluoride Film

Xiang Tao, Hao Jin*, Mengjuan Ma, Liwei Quan, Jinkai Chen, Shurong Dong, He Zhang, Chaofeng Lv, YongQing Fu, Jikui Luo

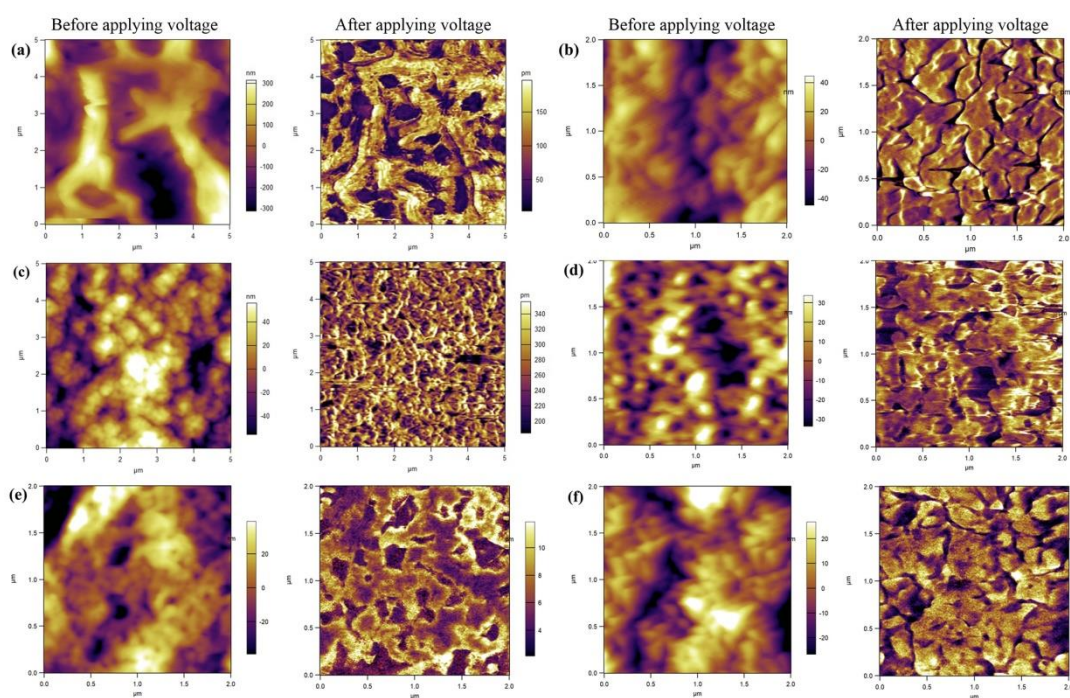


Figure S1. Surface topographies before and after applying voltage of PVDF-BTO films with 0 wt% (a) 5 wt% (b), 10 wt% (c), 15 wt% (d), 20 wt% (e), 30 wt% (f) BTO nanoparticles, respectively.

Table S1. d_0 of the TENGs in experiment

d_1 (μm)	ε_{r1}	d_2 (μm)	ε_{r2}	d_0 (μm)
60	4	20	19.2	16.04
60	4	36	19.2	16.87
60	4	50	19.2	17.60
60	4	80	19.2	19.17
60	4	100	19.2	20.21

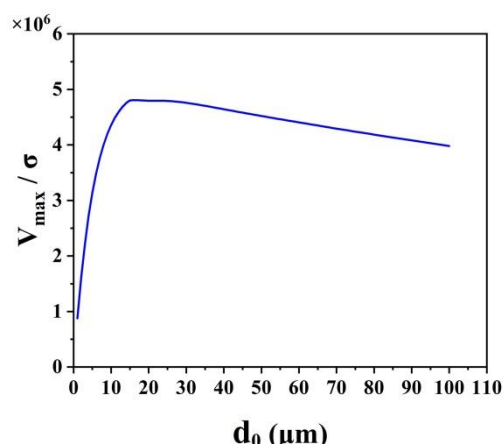
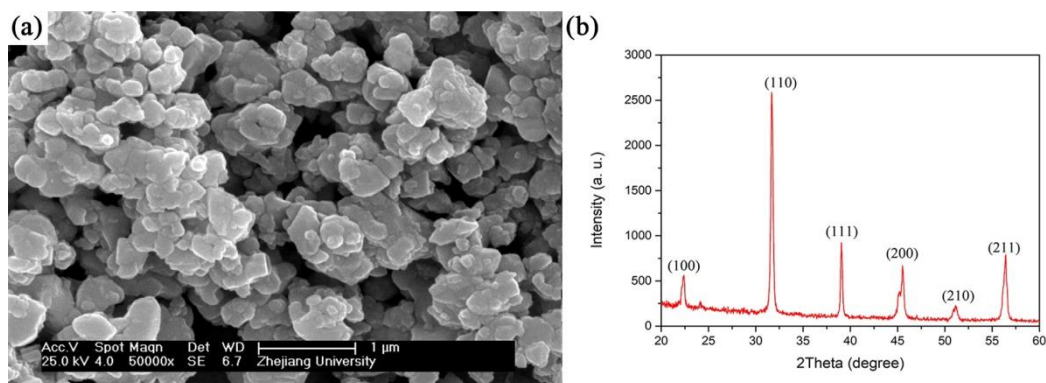
Figure S2. V_{\max}/σ of different effective thickness (d_0) of the TENG.

Figure S3. SEM photo (a) and X-Ray diffraction (XRD) pattern (b) of the BTO nanoparticles.